Supplemental Material for Local Markers for Crystalline Topology

Alexander Cerjan,[1,*] Terry A. Loring,[2] and Hermann Schulz-Baldes[3]

[1] *Center for Integrated Nanotechnologies, Sandia National Laboratories, Albuquerque, New Mexico 87185, USA*
[2] *Department of Mathematics and Statistics, University of New Mexico, Albuquerque, New Mexico 87131, USA*
[3] *FAU Erlangen-Nürnberg, Department Mathematik, Cauerstr. 11, D-91058 Erlangen, Germany*

SI. Properties of the symmetry-reduced spectral localizer

At the heart of the local topological invariant framework for crystalline symmetries developed in the main text are the spectral properties of the spectral localizer (Eq. (1) in the main text) which in the present situation is built from two Hermitian operators X and H on a Hilbert space $\mathcal{H}$ (called the position operator and Hamiltonian, respectively):

$$\begin{aligned} L_{(x,E)}(X,H) &= (H-E\mathbf{1})\otimes\sigma_x + \kappa(X-x\mathbf{1})\otimes\sigma_y \\ &= \begin{pmatrix} 0 & (H-E\mathbf{1}) - i\kappa(X-x\mathbf{1}) \\ (H-E\mathbf{1}) + i\kappa(X-x\mathbf{1}) & 0 \end{pmatrix}. \end{aligned}$$

Here σ_x, σ_y and σ_z are the three Pauli matrices, x, E are real numbers and $\kappa > 0$ is a tuning parameter that also guarantees consistent units. In general, one can build a spectral localizer from more Hermitian operators by using a larger-dimensional non-trivial Clifford representation. In order to compactify notations, we will simply drop the arguments X and H and write $L_{(x,E)} = L_{(x,E)}(X,H)$. In the present situation with two Hermitian operators X and H (or more generally an even number of them), the spectral localizer is odd with respect to the symmetry $\mathbf{1}\otimes\sigma_z$:

$$(\mathbf{1}\otimes\sigma_z)L_{(x,E)}(\mathbf{1}\otimes\sigma_z) = -L_{(x,E)}\ ,$$

so that it is off-diagonal in the grading of the Pauli matrices. Moreover, by construction the spectral localizer $L_{(x,E)}$ is Hermitian. These two properties imply that its spectrum is real and symmetric around 0. Note also that $L_{(x,E)}$ is invertible if and only if the off-diagonal entries are invertible. If invertibility is given, the signature $\mathrm{sig}[L_{(x,E)}]$ is well-defined. While $\mathrm{sig}[L_{(x,E)}]$ is useful for identifying material topology in the case of an odd number of Hermitian operators (corresponding to a physical system with even dimensionality) [1, 2], in the present situation it vanishes due to the symmetry of the spectrum.

It is possible, however, to extract important information from the spectral localizer if one has given another (unitary selfadjoint) symmetry operator $\mathcal{S}$ on $\mathcal{H}$ satisfying, just as in the main text,

$$\mathcal{S}^2 = \mathbf{1}, \qquad \mathcal{S} = \mathcal{S}^\dagger, \qquad \mathcal{S}H = H\mathcal{S}, \qquad \mathcal{S}X = -X\mathcal{S}. \tag{S1}$$

In the application in the main text, $\mathcal{S}$ is a crystalline symmetry, more precisely a reflection symmetry, but here we first consider general structural properties of the set-up given by (S1). The main point is the following conjugation with the unitary $\left(\begin{smallmatrix}\mathcal{S} & 0\\ 0 & \mathbf{1}\end{smallmatrix}\right)$ that can readily be checked:

$$\begin{pmatrix}\mathcal{S} & 0\\ 0 & \mathbf{1}\end{pmatrix}^\dagger L_{(x,E)} \begin{pmatrix}\mathcal{S} & 0\\ 0 & \mathbf{1}\end{pmatrix} = \begin{pmatrix} 0 & [((H-E\mathbf{1}) + i\kappa(X-x\mathbf{1}))\mathcal{S}]^\dagger \\ ((H-E\mathbf{1}) + i\kappa(X-x\mathbf{1}))\mathcal{S} & 0 \end{pmatrix}. \tag{S2}$$

This unitary equivalence shows that the operator on the r.h.s. has the same spectrum as $L_{(x,E)}$. In general, the off-diagonal blocks on the r.h.s. of Eq. (S2) are non-Hermitian, but the commutation relations (S1) imply that they *are* Hermitian at $x = 0$. Hence let us introduce the symmetry-reduced or $\mathcal{S}$-reduced spectral localizer $\tilde{L}^{\mathcal{S}}_E = \tilde{L}^{\mathcal{S}}_E(X,H)$ by

$$\tilde{L}^{\mathcal{S}}_E \ = \ ((H-E\mathbf{1}) + i\kappa X)\mathcal{S}\ .$$

The terminology reflects that $\tilde{L}^{\mathcal{S}}_E$ depends on the symmetry $\mathcal{S}$ and consists only of one block entry of the spectral localizer, and is hence reduced. However, as stated above, the relations (S1) imply that it is nevertheless Hermitian

* awcerja@sandia.gov

and clearly one has

$$\begin{pmatrix} \mathcal{S} & 0 \\ 0 & \mathbf{1} \end{pmatrix}^\dagger L_{(0,E)} \begin{pmatrix} \mathcal{S} & 0 \\ 0 & \mathbf{1} \end{pmatrix} = \begin{pmatrix} 0 & \tilde{L}_E^{\mathcal{S}} \\ \tilde{L}_E^{\mathcal{S}} & 0 \end{pmatrix}. \tag{S3}$$

It is possible to rewrite the $\mathcal{S}$-reduced spectral localizer in a form that looks more like in other works. For that purpose, let us split the Hilbert space $\mathcal{H}$ into even and odd elements w.r.t. $\mathcal{S}$:

$$\mathcal{H} = \mathcal{H}_+ \oplus \mathcal{H}_-, \qquad \mathcal{H}_\pm = \big\{\psi \in \mathcal{H} \,:\, \mathcal{S}\psi = \pm\psi\big\}.$$

Now $H : \mathcal{H}_\pm \to \mathcal{H}_\pm$ leaves subspaces invariant and can thus be decomposed as $H = H_+ \oplus H_-$. On the other hand, $X : \mathcal{H}_\pm \to \mathcal{H}_\mp$ is off-diagonal in the grading of $\mathcal{S}$ and thus let us use the notation $\tilde{X} = X|_{\mathcal{H}_+} : \mathcal{H}_+ \to \mathcal{H}_-$ for the restriction of X. Then in the grading of $\mathcal{S}$:

$$\tilde{L}_E^{\mathcal{S}} = \begin{pmatrix} (H_+ - E\mathbf{1}_+) & -i\kappa\tilde{X}^\dagger \\ i\kappa\tilde{X} & -(H_- - E\mathbf{1}_-) \end{pmatrix}, \tag{S4}$$

where $\mathbf{1}_\pm$ is the identity on $\mathcal{H}_\pm$. This resembles the even spectral localizer in [2], in particular in the general form of [3] where also not necessarily all components of the position operator enter into the construction. Another crucial property is that its square

$$(\tilde{L}_E^{\mathcal{S}})^2 \;=\; (H - E\mathbf{1})^2 + i\kappa[X,H]\mathcal{S} + \kappa^2 X^2 \tag{S5}$$

only involves the commutator $[X,H]$ and *not* a term like $XH + HX$. In applications to local operators, $[X,H]$ is uniformly bounded, but $XH + HX$ grows with the volume. Also note that $i\kappa[X,H]\mathcal{S}$ is a Hermitian operator which is odd w.r.t. $\mathcal{S}$, namely $\mathcal{S}^\dagger\big(i\kappa[X,H]\mathcal{S}\big)\mathcal{S} = -\big(i\kappa[X,H]\mathcal{S}\big)$.

For any Hermitian A, the spectrum of $\left(\begin{smallmatrix} 0 & A \\ A & 0 \end{smallmatrix}\right)$ consists of the union of the spectrum of A with its negative because, if $A\psi = \lambda\psi$, the two eigenvectors of $\left(\begin{smallmatrix} 0 & A \\ A & 0 \end{smallmatrix}\right)$ are simply $\left(\begin{smallmatrix} \pm\psi \\ \psi \end{smallmatrix}\right)$. Thus

$$\lambda \text{ or } -\lambda \text{ is an eigenvalue of } \tilde{L}_E^{\mathcal{S}} \quad\Longleftrightarrow\quad \pm\lambda \text{ are both eigenvalues of } L_{(0,E)}. \tag{S6}$$

Another piece of spectral information of an arbitrary linear operator A is its invertibility gap $\mu(A) \geq 0$ defined by

$$\mu(A) = \min\big\{\sqrt{|\lambda|} \,:\, \lambda \in \mathrm{spec}(A^\dagger A)\big\} = \sqrt{\mu(A^\dagger A)}.$$

For matrices, $\mu(A)$ is also called the smallest singular value. If $A^\dagger = A$ is a Hermitian matrix (or more generally A is normal, namely $AA^\dagger = A^\dagger A$), then $\mu(A)$ is the smallest of all absolute values of the eigenvalues of A. For the spectral localizer, let us introduce the notation

$$\mu_{(x,E)} = \mu_{(x,E)}(X,H) = \mu(L_{(x,E)}(X,H)).$$

Then (S6) implies

$$\mu_{(0,E)} = \mu(L_{(0,E)}) = \mu(\tilde{L}_E^{\mathcal{S}}) = \mu\big((H - E\mathbf{1}) + i\kappa X\big). \tag{S7}$$

In the following, let us suppose that the Hilbert space $\mathcal{H}$ is finite dimensional which is relevant for the numerical treatment in the main text. Whenever $\mu_{(0,E)} > 0$, one can define

$$\zeta_E^{\mathcal{S}} = \tfrac{1}{2}\,\mathrm{sig}[\tilde{L}_E^{\mathcal{S}}],$$

which is an integer/half-integer if the dimension of the Hilbert space is even/odd. Changes of the half-signature are always integer and actually define the spectral flow through 0, see Section 1 in [4]:

$$\mathrm{Sf}\big(E \in [E_0, E_1] \mapsto \tilde{L}_E^{\mathcal{S}}\big) = \tfrac{1}{2}\big(\mathrm{sig}[\tilde{L}_{E_1}^{\mathcal{S}}] - \mathrm{sig}[\tilde{L}_{E_0}^{\mathcal{S}}]\big) = \zeta_{E_1}^{\mathcal{S}} - \zeta_{E_0}^{\mathcal{S}}, \tag{S8}$$

provided that $\tilde{L}_{E_1}^{\mathcal{S}}$ and $\tilde{L}_{E_0}^{\mathcal{S}}$ are invertible. Hence it is natural to consider the jump (or discontinuity or critical) points E_c of the function $E \mapsto \zeta_E^{\mathcal{S}}$ which are precisely the points at which there is spectral flow. These points E_c can also

be characterized as those points E_c for which $\mathrm{Ker}(\tilde{L}^{\mathcal{S}}_{E_c})$ is non-trivial. The following proposition shows that in the vicinity of such jump points E_c there must be an element in the spectrum of H.

Proposition 1. *Suppose $E_c \in \mathbb{R}$ is such that the dimension $m_c = \dim(\mathrm{Ker}(\tilde{L}^{\mathcal{S}}_{E_c}))$ is positive. Then H has at least m_c eigenvalues in $[E_c - \sqrt{\kappa\,\|[X,H]\|}, E_c + \sqrt{\kappa\,\|[X,H]\|}]$, counted with their multiplicity.*

Proof. By Courant's minmax principle it is sufficient to show that there is an m_c-dimensional subspace $\mathcal{E}_c$ of the Hilbert space such that $\kappa\|[X,H]\| - (H - E_c\mathbf{1})^2 \geq 0$ in the sense of positive operators. This will be verified for $\mathcal{E}_c = \mathrm{Ker}(\tilde{L}^{\mathcal{S}}_{E_c})$. Indeed, for the restrictions on this subspace one has

$$0 = (\tilde{L}^{\mathcal{S}}_{E_c})^2\big|_{\mathcal{E}_c} = \big((H - E_c\mathbf{1})^2 + i\kappa[X,H]\mathcal{S} + \kappa^2 X^2\big)\big|_{\mathcal{E}_c} \geq \big((H - E_c\mathbf{1})^2 - \kappa\|[X,H]\|\big)\big|_{\mathcal{E}_c}\,,$$

just as required. □

Proposition 1 does *not* exclude that there are further eigenvalues of H in $[E_c - \sqrt{\kappa\,\|[X,H]\|}, E_c + \sqrt{\kappa\,\|[X,H]\|}]$. For example, in Fig. 1 in the main there is a kernel of dimension m_c at $\omega = 0.5152(2\pi c/a)$, but besides an eigenvalue of H at precisely this energy, there are certainly two further eigenvalues of H in a small interval around it (at $\omega = 0.5121(2\pi c/a)$ and $\omega = 0.5125(2\pi c/a)$) that correspond to edge-localized states, see Sec. SVII. Nevertheless, only the state at $\omega = 0.5152(2\pi c/a)$ is a corner state, as can readily be seen by looking at the plots in Fig. S5 of the field intensity $|E_z|^2$ of the two other eigenfunctions.

Let us outline a numerical procedure for how to isolate the topological boundary state corresponding to a jump of $E \mapsto \zeta^{\mathcal{S}}_E$ at E_c by $+1$ and with $m_c = 1$ which is the generic case (as higher degeneracies of the kernel are lifted by a generic symmetry-preserving perturbation). This may be of help in simulations at large volume when there are many eigenstates of H close to E_c.

1. First choose an interval $[E_c - \delta, E_c + \delta]$ for a small $\delta > 0$ such that the interval contains an odd number of eigenvalues with normalized eigenstates $\boldsymbol{\psi}_1, \ldots, \boldsymbol{\psi}_{2n+1}$ of H, but no other E with $\mu_{(0,E)} = 0$. Order them such that the states with positive $\mathcal{S}$-parity are listed first. There should be $n+1$ states with positive $\mathcal{S}$-parity and n with negative $\mathcal{S}$-parity (if this is not the case, one may have "just missed" one state and should slightly enlarge δ; of course, δ should chosen sufficiently small so that n is not too large).

2. Then introduce the frame $\Psi = (\boldsymbol{\psi}_1, \ldots, \boldsymbol{\psi}_{2n+1})$, which decomposes to $\Psi = (\Psi_+, \Psi_-)$ with $\mathcal{S}\Psi_\pm = \pm\Psi_\pm$. Hence Ψ_+ and Ψ_- are of dimension $n+1$ and n respectively. One of the $n+1$ states in Ψ_+ is the topological boundary state. Introduce two diagonal matrices $E_\pm$ (of dimension $n+1$ and n) such that $H\Psi_\pm = \Psi_\pm E_\pm$.

3. Then taking matrix element of (S4) leads to

$$\Psi^\dagger \tilde{L}^{\mathcal{S}}_E \Psi = \begin{pmatrix} E_+ - E\mathbf{1}_+ & -i\kappa(\Psi_+)^\dagger X \Psi_- \\ i\kappa(\Psi_-)^\dagger X \Psi_+ & -(E_- - E\mathbf{1}_-) \end{pmatrix}, \tag{S9}$$

   where the identities $\mathbf{1}_\pm$ are of dimension $n+1$ and n. Now compute the $(n+1)\times n$ matrix $(\Psi_+)^\dagger X \Psi_-$ numerically.

4. There should be one line which is considerably smaller than all others. Shift the corresponding eigenvector into the first row of Ψ, then $\boldsymbol{\psi}_1 = \boldsymbol{\psi}_b$ is the desired topological boundary state with eigenvalue E_b, namely $H\boldsymbol{\psi}_b = E_b\boldsymbol{\psi}_b$. Supposing that $(\boldsymbol{\psi}_b)^\dagger X \Psi_-$ even vanishes (as it is really negligible compared to the rest), then the first row and first column of $\Psi^\dagger \tilde{L}^{\mathcal{S}}_E \Psi$ vanishes, except for the entry $(1,1)$ which is $E_b - E$, and hence this eigenvalue is effectively decoupled from all other states. Of the remaining entries of $(\Psi_+)^\dagger X \Psi_-$ there may be many of order 1, and these then move the eigenvalues of $\tilde{L}^{\mathcal{S}}_E$ out of the kernel, provided that κ is larger than the diagonal entries. This also explains why it is *not advantageous* to choose κ too small, see Sec. SIII for further discussion.

5. Once the topological boundary state $\boldsymbol{\psi}_b$ is determined, one now has

$$(\boldsymbol{\psi}_b)^\dagger \tilde{L}^{\mathcal{S}}_E \boldsymbol{\psi}_b \approx E_b - E + \mathcal{O}(\kappa),$$

   where the order κ correction term results from the coupling with other states (also those not included in Ψ). In particular, the energy E_c with non-trivial kernel of $\tilde{L}^{\mathcal{S}}_E$ satisfies

$$E_b - E_c = \mathcal{O}(\kappa),$$

which is considerably better than the estimate of Proposition 1 which only provides $E_b - E_c = \mathcal{O}(\sqrt{\kappa})$.

6. If the jump of $\zeta_E^{\mathcal{S}}$ at E_c would be -1 (namely the spectral flow would be -1), the same argument as above can be applied, except that $\boldsymbol{\psi}_b$ would be of negative $\mathcal{S}$-parity $s_b = -1$. As the sign in the lower right entry in (S9) is different, this leads to a sign change. In both cases, one therefore has (see eq. (10) in the main text)

$$(\boldsymbol{\psi}_b)^\dagger \tilde{L}_E^{\mathcal{S}} \boldsymbol{\psi}_b \approx s_b(E_c - E) + \mathcal{O}(\kappa). \tag{S10}$$

It is possible to add some mathematical rigor to the argument leading to (S10), even in the case of Proposition 1 where m_c is larger than 1, but only for κ very small. The reasoning will analyze the dependence of $\tilde{L}_E^{\mathcal{S}}$ on both E and κ, and therefore it will rather be denoted by $\tilde{L}_{\kappa,E}^{\mathcal{S}}$, and similarly $\zeta_{\kappa,E}^{\mathcal{S}}$. The most important property of the matrix-valued function $(\kappa, E) \in \mathbb{R}^2 \mapsto \tilde{L}_{\kappa,E}^{\mathcal{S}}$ is that it is real analytic in both variables with values in the Hermitian matrices. Therefore Kato's analytic perturbation theory applies [5], both to $\tilde{L}_{\kappa,E}^{\mathcal{S}}$ as well as $(\tilde{L}_{\kappa,E}^{\mathcal{S}})^2$ given in (S5). In particular, for a given δ (that will be chosen to be smaller or of the order of κ), one can look at the spectral projection $P_{\kappa,E}^{\delta} = \chi(\tilde{L}_{\kappa,E}^{\mathcal{S}} \in (-\delta, \delta))$ of $\tilde{L}_{\kappa,E}^{\mathcal{S}}$ onto the interval $(-\delta, \delta)$. As long as its dimension is constant, is then known to depend analytically on κ and E.

Proposition 2. *Suppose that for given (κ, E_c) one has $m_c = \dim(\mathrm{Ker}(\tilde{L}_{\kappa,E_c}^{\mathcal{S}})) > 0$. Moreover, suppose that there is a $\delta > 0$ such the $\kappa' \in [0, \kappa] \mapsto P_{\kappa',E_c}^{\delta}$ has constant dimension equal to m_c. Then the ζ-jump at E_c (or equivalently the spectral flow of the $\mathcal{S}$-reduced spectral localizer at E_c) is given by the sum of the $\mathcal{S}$-parities $s_j \in \{-1, 1\}$, $j = 1, \ldots, m_c$, of the m_c eigenstates of H with energies in the spectral interval $[E_c - \delta, E_c + \delta]$:*

$$\lim_{\epsilon \to 0} \zeta_{\kappa,E_c+\epsilon}^{\mathcal{S}} - \zeta_{\kappa,E_c-\epsilon}^{\mathcal{S}} = -\mathrm{sig}\big[\mathcal{S}|_{\mathrm{Ran}(P_{0,E_c}^{\delta})}\big] = -\sum_{j=1}^{m_c} s_j,$$

where $\mathcal{S}|_{\mathrm{Ran}(P_{0,E_c}^{\delta})}$ denotes the restriction of the quadratic form $\mathcal{S}$ to the range of the projection P_{0,E_c}^{δ}.

Proof. Due to (S8), the desired ζ-jump is given given by the spectral flow of the $\mathcal{S}$-reduced spectral localizer at E_c. Moreover, it is well-known that this spectral flow can be computed via the signature of the so-called crossing form [4]. Together, one gets for ϵ sufficiently small:

$$\zeta_{\kappa,E_c+\epsilon}^{\mathcal{S}} - \zeta_{\kappa,E_c-\epsilon}^{\mathcal{S}} = \mathrm{Sf}\big(E \in [E_c - \epsilon, E_c + \epsilon] \mapsto \tilde{L}_{\kappa,E}^{\mathcal{S}}\big) = \mathrm{sig}\Big[\partial_E \tilde{L}_{\kappa,E}^{\mathcal{S}}\big|_{\mathrm{Ker}(\tilde{L}_{\kappa,E_c}^{\mathcal{S}})}\Big].$$

The derivative can readily be read off from the definition of $\tilde{L}_{\kappa,E}^{\mathcal{S}}$:

$$\zeta_{\kappa,E_c+\epsilon}^{\mathcal{S}} - \zeta_{\kappa,E_c-\epsilon}^{\mathcal{S}} = \mathrm{sig}\Big[-\mathcal{S}\big|_{\mathrm{Ker}(\tilde{L}_{\kappa,E_c}^{\mathcal{S}})}\Big] = -\mathrm{sig}\Big[\mathcal{S}\big|_{\mathrm{Ker}(\tilde{L}_{\kappa,E_c}^{\mathcal{S}})}\Big].$$

Now one has $\mathrm{Ker}(\tilde{L}_{\kappa,E_c}^{\mathcal{S}}) = \mathrm{Ran}(P_{\kappa,E_c}^{\delta})$. By assumption and analytic perturbation theory, there is a constant such that $\|P_{\kappa,E_c}^{\delta} - P_{0,E_c}^{\delta}\| \leq C\kappa$. As the spectrum of $\mathcal{S}$ restricted to $\mathrm{Ran}(P_{0,E_c}^{\delta})$ is contained in $\{-1, 1\}$, this implies that also $\mathcal{S}$ restricted to $\mathrm{Ran}(P_{\kappa',E_c}^{\delta})$ is invertible for all $\kappa' \in [0, \kappa]$. Consequently, the signature of these restrictions does not change and one concludes

$$\zeta_{\kappa,E_c+\epsilon}^{\mathcal{S}} - \zeta_{\kappa,E_c-\epsilon}^{\mathcal{S}} = -\mathrm{sig}\Big[\mathcal{S}\big|_{\mathrm{Ran}(P_{\kappa,E_c}^{\delta})}\Big] = -\mathrm{sig}\Big[\mathcal{S}\big|_{\mathrm{Ran}(P_{0,E_c}^{\delta})}\Big].$$

Finally, $\tilde{L}_{0,E_c}^{\mathcal{S}} = (H - E_c\mathbf{1})\mathcal{S}$ and therefore $\mathrm{Ran}(P_{0,E_c}^{\delta})$ is spanned by the eigenstates $\boldsymbol{\psi}_1, \ldots, \boldsymbol{\psi}_{m_c}$ of H with energies lying in $[E_c - \delta, E_c + \delta]$. These states have $\mathcal{S}$-parties $s_j \in \{-1, 1\}$ given by $\mathcal{S}\boldsymbol{\psi}_j = s_j\boldsymbol{\psi}_j$ for $j = 1, \ldots, m_c$. Replacing this implies the claim. □

SII. Homotopy characterization for finite systems

This section proves the claim from the main text (see the discussion after Eq. (4)) that $\zeta_E^{\mathcal{S}}$ classifies pairs (X, H) of selfadjoint matrices satisfying $\mathcal{S}H = H\mathcal{S}$ and $\mathcal{S}X = -X\mathcal{S}$. The same argument applies to chiral Hamiltonians $JHJ = -H$ for some selfadjoint involution J commuting with another selfadjoint matrix X if one uses the chiral spectral localizer $\tilde{L}^J(X, H) = (\kappa X + iH)J$ as in [6]. Hence let us take a more general set-up. Suppose given a

finite-dimensional Hilbert space equipped with a fixed selfadjoint unitary Π. For two Hermitian matrices A and B on this Hilbert space satisfying with $A\Pi = \Pi A$ and $B\Pi = -\Pi B$, let us use the Π-reduced spectral localizer

$$\tilde{L}^{\Pi}(A, B) = (A + iB)\,\Pi.$$

Lemma 3. *Suppose given two matrices A_j and B_j, $j = 0, 1$, satisfying*

$$A_j\Pi = \Pi A_j \quad \text{and} \quad B_j\Pi = -\Pi B_j,$$

and further suppose that both associated reduced spectral localizers are gapped:

$$\min\left(\tilde{L}^{\Pi}(A_j, B_j)\right) \geq \delta > 0.$$

There exists a continuous path of matrices $t \in [0, 1] \mapsto (A_t, B_t)$ connecting (A_0, B_0) to (A_1, B_1) and satisfying

$$A_t\Pi = \Pi A_t \quad \text{and} \quad B_t\Pi = -\Pi B_t \quad \text{and} \quad \mu\left(\tilde{L}^{\Pi}\left(A_t, B_t\right)\right) \geq \delta,$$

if, and only if,

$$\operatorname{sig}\left[\tilde{L}^{\Pi}(A_0, B_0)\right] = \operatorname{sig}\left[\tilde{L}^{\Pi}(A_1, B_1)\right].$$

Proof. If such a path exists, then the path $\tilde{L}^{\Pi}(A_t, B_t)$ is a continuous path of invertible Hermitian matrices, along which the signature cannot change. The key to proving the converse is to use the formulas that take us from $\tilde{L}^{\Pi}(A, B)$ back to A and B. These are

$$A = \frac{1}{2}\left(\left(\tilde{L}^{\Pi}(A, B)\Pi\right)^{\dagger} + \tilde{L}^{\Pi}(A, B)\Pi\right), \qquad B = \frac{i}{2}\left(\left(\tilde{L}^{\Pi}(A, B)\Pi\right)^{\dagger} - \tilde{L}^{\Pi}(A, B)\Pi\right).$$

The matrices $\tilde{L}^{\Pi}(A_0, B_0)$ and $\tilde{L}^{\Pi}(A_1, B_1)$ are by assumption Hermitian, gapped and have the same signature. By a straightforward argument based on the spectral theorem (diagonalize with diagonal entries ordered to their size, linearly interpolate between the diagonal matrices, finally deform the unitaries using their matrix logarithm), there exists a continuous path $t \in [0, 1] \mapsto L_t$ of invertible selfadjoints connecting $L_0 = \tilde{L}^{\Pi}(A_0, B_0)$ to $L_1 = \tilde{L}^{\Pi}(A_1, B_1)$. Then set

$$A_t = \frac{1}{2}\left((L_t\Pi)^{\dagger} + L_t\Pi\right), \qquad B_t = \frac{i}{2}\left((L_t\Pi)^{\dagger} - L_t\Pi\right).$$

These are clearly continuous paths of Hermitian matrices. Also, as required

$$2\Pi A_t = L_t + \Pi L_t\Pi = 2A_t\Pi, \qquad -2i\Pi B_t = L_t - \Pi L_t\Pi = 2iB_t\Pi.$$

Finally

$$\tilde{L}^{\Pi}(A_t, B_t) = \frac{1}{2}\left((\Pi L_t + L_t\Pi)\,\Pi - (\Pi L_t - L_t\Pi)\,\Pi\right) = L_t$$

so the path is in the invertibles as required. □

While the previous lemma provides the desired classification, the result can probably be strengthened. It should be possible that along the constructed path $t \mapsto (A_t, B_t)$ the locality of the operators can be preserved as physical intuition suggests. One way to approach the problem is to realize that the commutator $[A, B]$ of the two Hermitian matrices can be made arbitrarily small by choosing the tuning parameter κ small (recall that $A = H$, $B = \kappa X$ and $\Pi = \mathcal{S}$ in the situation of the main text). Then Lin's theorem [7] states that there are nearby Hermitian operators A' and B' which commute. This allows to construct a short part connecting them which hence conserves locality, as pointed out in [8]. It is an interesting open question whether one can generalize Lin's theorem by guaranteeing that A' and B' satisfy the same symmetry relations $A'\Pi = \Pi A'$ and $B'\Pi = -\Pi B'$. We conjecture that this is true, given that similar statements have been proven for matrix symmetries corresponding to Altland-Zirnbauer symmetry classes AI and AII [9] as well as classes C and D [10].

SIII. The scaling coefficient κ

The scaling coefficient κ serves two roles in the spectral localizer: it guarantees consistent units between the two constituent operators, the position operators on one side and the Hamiltonian on the other, and it adjusts the effective weighting between these operators in the spectral localizer's spectrum. The tuning of κ is crucial because the two limiting cases $\kappa \downarrow 0$ and $\kappa \uparrow \infty$ both yield objects of no interest. For $\kappa = 0$, the spectrum of $L_{(x,E)}$ is simply related to the spectrum of the underlying Hamiltonian, and thus the spectral localizer provides no additional information. Similarly, for $\kappa \uparrow \infty$, $L_{(x,E)}$ only reveals the distribution of the system's sites. Instead, for the spectral localizer to provide new and useful information about a system, κ needs to be chosen to neither be too large nor too small. These comments directly transpose the symmetry-reduced spectral localizer $\tilde{L}_E^S$ due to Eqs. (S3) and (S6).

The spectral localizer in several prior works [1, 2, 11] is used to compute the bulk topological invariants for bulk tight-binding Hamiltonians H_{bulk} that fall within one of the ten Altland-Zirnbauer classes [12–14]. In this context, there are proven bounds on κ that guarantee that the spectral localizer is gapped (i.e. $\mu \neq 0$) so that its signature is a well-defined and stable quantity. More precisely, let E be the energy where the system's topology is being evaluated, let g be the size of the band gap of H_{bulk} around that E, and l the length from the center of the sample to the boundary of the finite system. Then the bounds

$$\kappa \leq \frac{g^3}{12\|H_{\text{bulk}} - E\mathbf{1}\| \left(\sum_{j=1}^{d} \|[X_j, H_{\text{bulk}}]\|\right)}, \tag{S11}$$

$$\kappa \geq \frac{2g}{l}, \tag{S12}$$

guarantee that the gap of the spectral localizer $L_{(0,E)}$ around 0 is at least $\frac{g}{2}$ (see Theorem 2 of Ref. [2] and Chapter 10 in [4]). Due to Eq. (S3) this again transposes directly to the symmetry-reduced spectral localizer. Let us stress that the result makes no other assumption on the Hamiltonian H_{bulk} than the existence of a spectral gap. The Hamiltonian need not be periodic or otherwise be homogeneous in space (such as in a quasicrystal). In particular, the result also holds for Hamiltonians describing defects. However, if a Hamiltonian describing a defect has a boundary state at energy E, then the spectral gap g vanishes at that energy and necessarily the gap of spectral localizer also vanishes. Hence, in this work, there is a shift of perspective on the spectral localizer (or rather its symmetry-reduced cousin) relative to these prior studies [1, 2, 11]: it is not only used to detect (bulk) topological invariants, but also to localize topological bound states. In the following, we argue that for the purpose of detecting these boundary-localized states, an adequate choice for the size of κ is nevertheless given by Eq. (S12) if g is chosen to be the bulk gap.

Before going on though, let us stress that the bounds on the gap of the spectral localizer are not available for unbounded Hamiltonians, such as for photonic systems where Maxwell's equation leads to an unbounded Hamiltonian. In particular, the hypothesis (S11) is meaningless for unbounded Hamiltonians where $\|H_{\text{bulk}}\| \to \infty$. To recover a useful bound this quantity needs to be made finite in some way. One possibility is to use the resolvent $\|H_{\text{bulk}}\| \to \|(H_{\text{bulk}} - E\mathbf{1})^{-1} H_{\text{bulk}}\|$ (which would still need to have its units corrected in some appropriate manner). Another possibility is to project into the local-in-energy subspace $\|H_{\text{bulk}}\| \to \|\Psi^\dagger H_{\text{bulk}} \Psi\|$ where Ψ is rectangular matrix whose m columns are the eigenvectors of the m eigenvalues of H_{bulk} closest to the chosen E [15]. However, at present, it is not known how either of these changes will alter the bounds, or if there is an entirely different, better approach.

Nevertheless, Eq. (S12) is expressed in terms of quantities that can still be calculated for a system with an unbounded Hamiltonian. This connection (S12) is used as a guiding principle for the choice of κ with g being the bulk gap (and *not* the energetic distance from E to the boundary-localized state). For the system shown in Fig. 1 of the main text, the bulk gap is $g \approx 0.068(2\pi c)^2/a^2$ and the length of the system in y is $l = 8.65a$, yielding $\kappa \approx 0.016(2\pi c)^2/a^3$. As can be seen, this is very similar to the value of $\kappa = 0.010(2\pi c)^2/a^3$ used in those simulations.

By direct calculation, we confirm that κ can be varied by over an order of magnitude while yielding quantitatively similar results. In Fig. S1, we show the local gap and local index for a range of κ surrounding the value predicted by Eq. (S12). The three central panels, $\kappa = [0.002,\ 0.010,\ 0.030](2\pi c)^2/a^3$ all show nearly the same quantitative results, with two topological corner modes within the bulk band gap identified by a closing in the local gap where the local index also changes. The leftmost ($\kappa = 0.001(2\pi c)^2/a^3$) and rightmost ($\kappa = 0.040(2\pi c)^2/a^3$) panels both show how the theory begins to break down. For too small a κ, too many states are identified as topological in the system; in this case, two nearly degenerate edge-localized modes are identified as topological. Similarly, when κ is too large, one of the in-gap topological corner states is effectively combined with an in-band state with the opposite topological charge.

Heuristically, the behavior seen in Fig. S1 is demonstrating that the effect of κ is to smooth out pairs of nearly

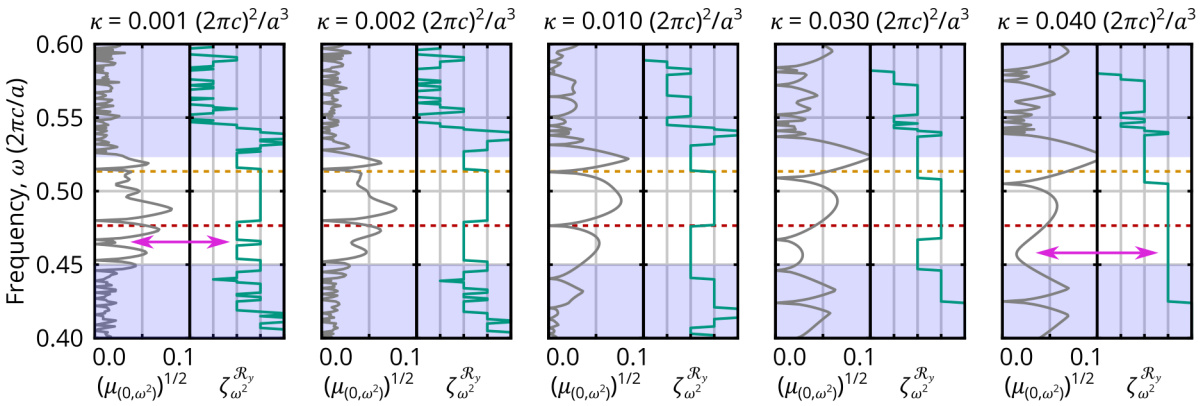

FIG. S1. Local gap $(\mu_{(0,\omega^2)})^{(1/2)}$ in units of $2\pi c/a$ (left panels) and local index $\zeta^{\mathcal{R}_y}_{\omega^2}$ (right panels) calculated using the value of κ indicated above each pair of panels for the system shown in Fig. 1 of the main text. The middle panel reproduces the data from Fig. 1(c) and (d). The shaded regions demarcate those spectral regions where states can exist in the crystalline bulk. For $\kappa = 0.001(2\pi c)^2/a^3$, the magenta arrow indicates where the local index is changing for a pair of edge states. For $\kappa = 0.040(2\pi c)^2/a^3$, the magenta arrow indicates where a corner state is no longer associated with a change in the local index.

degenerate modes with opposite symmetry, removing their presence from the local gap and local index. In this case, the in-gap nearly degenerate modes are made of edge-localized states that form an even and odd pair with respect to the reflection symmetry at the corner, whose frequencies are guaranteed to be similar, but distinct. However, if κ is too large, some of the corner-localized modes are smoothed out with their in-band even/odd partner. This argument confirms the prediction that κ should be both related to the gap size, which determines how far away such an in-band even/odd partner state is in energy, as well as the finite system's size, which sets the energy scale of the even-odd splitting between the edge-localized states (larger l reduces the edge state splitting).

SIV. Additional details on the perturbed corner heterostructure

In Fig. 1 of the main text, the local gap is seen to indicate that the higher-frequency corner-localized state has more topological protection than the lower-frequency corner state, despite being closer-in-frequency to one of the bulk bands. Here, we provide additional simulation results beyond those shown in Fig. 2 of the main text to support the conclusions discussed in conjunction with that figure.

In Fig. S2 we consider the same two perturbation distributions as considered in the main text, tailored to affect either the lower-frequency corner state [Fig. S2(a)] or the higher-frequency corner state [Figs. S2(b),(c)], with the field profiles of these states in the unperturbed system shown in Fig. 1(e) of the main text. The total perturbation is then the perturbation strength $\delta\varepsilon \in \mathbb{R}$ multiplied by the perturbation distribution $u(\mathbf{x})$, i.e. $\delta\varepsilon_{\text{tot}}(\mathbf{x}) = \delta\varepsilon\, u(\mathbf{x})$. The two chosen perturbation distributions have similar overlaps with their respective modes, the higher-frequency corner state modal overlap is $\int E^*_{z,\text{hf}}(\mathbf{x})u_{\text{hf}}(\mathbf{x})E_{z,\text{hf}}(\mathbf{x})d\mathbf{x} = 0.07 = \bar{u}_{\text{hf}}$, while the lower-frequency corner state modal overlap is $\int E^*_{z,\text{lf}}(\mathbf{x})u_{\text{lf}}(\mathbf{x})E_{z,\text{lf}}(\mathbf{x})d\mathbf{x} = 0.12 = \bar{u}_{\text{lf}}$. Here, $u_{\text{lf}}(\mathbf{x})$ is shown in Fig. S2(a), and $u_{\text{hf}}(\mathbf{x})$ in Figs. S2(b) or (c), while the modal fields $E_z(\mathbf{x})$ of bound states of the unperturbed system are shown in Fig. 1(e) of the main text.

To demonstrate that the topological phase transitions are happening at the perturbation strengths claimed in the main text, in Fig. S2 we show closely spaced perturbation strengths on either side of the topological transition. In each case, the relevant topological that disappears as the perturbation strength is slightly increased is marked by the magenta arrow. In Fig. S2(c), we also show the possibility of attempting to merge the two in-gap corner states, as opposed to combining them with states from the bulk bands as is considered in Figs. S2(a) and (b). From Fig. 1(d), the local gap reveals that the topological protection of the lower-frequency corner state against merging with the lower-frequency bulk band is less than that of merging the two in-gap states together, which is again less than that of merging the higher-frequency corner state with the higher-frequency bulk band. This is because the maximum local gap attained over frequencies below the lower-frequency corner mode is less than the maximum local gap for frequencies in between the two corner states, which is again less than the local gap for frequencies greater than the

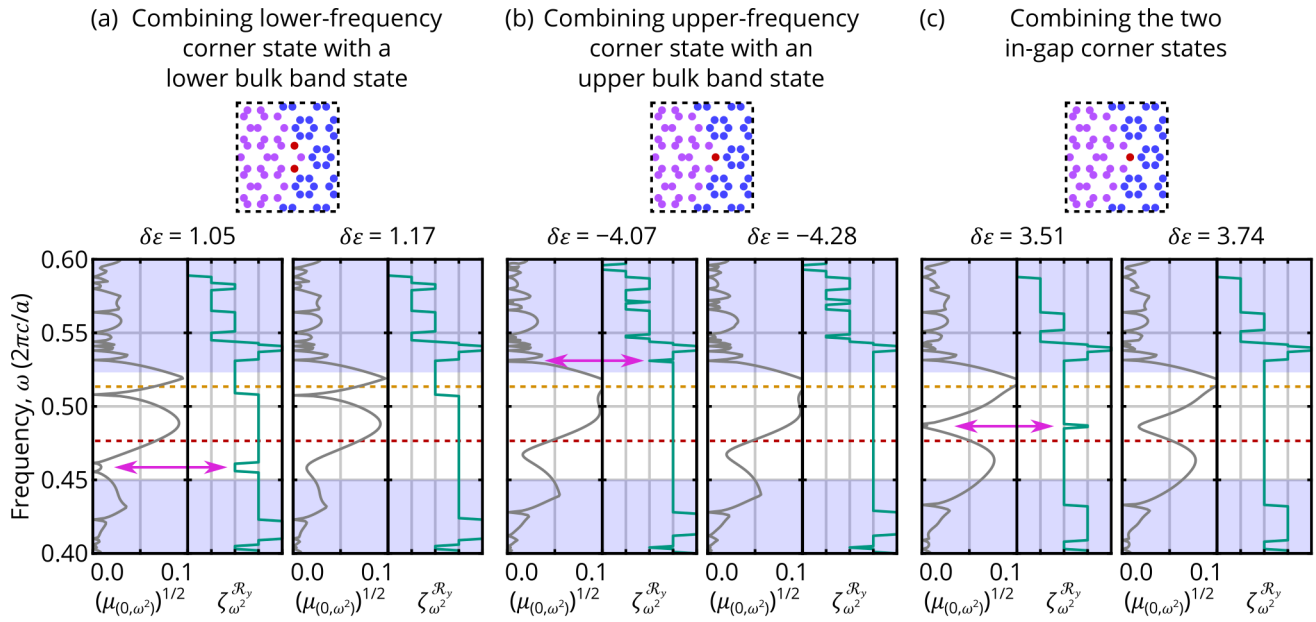

FIG. S2. Studies of three different perturbations designed to annihilate one or both of the original in-gap topological corner states by combining the state with an opposite-symmetry partner. The top row shows zoomed-in diagrams of the perturbation's distribution (red) in the overall photonic corner heterostructure from Fig. 1 in the main text. The bottom left panel for each case shows the local gap $(\mu_{(0,\omega^2)})^{(1/2)}$ in units of $2\pi c/a$ and local index $\zeta_{\omega^2}^{\mathcal{R}_y}$ calculated using $\kappa = 0.01(2\pi c)^2/a^3$ for a perturbation strength just below the strength at which the topological corner mode is annihilated. The bottom right panel shows the same quantities for a perturbation strength just above the strength at which the topological corner mode is annihilated. The magenta arrow indicates the topological feature that disappears as the perturbation strength is increased. The shaded regions demarcate those spectral regions where states can exist in the crystalline bulk. (a) The perturbation is chosen to combine: (a) the lower-frequency corner state with a state from the lower-frequency bulk band; (b) the higher-frequency corner state with a state from the higher-frequency bulk band; (c) the two in-gap corner-localized states.

higher-frequency corner state,

$$\max_{\omega<\omega_{\rm lf}} \mu_{(0,\omega^2)} < \max_{\omega_{\rm lf}<\omega<\omega_{\rm uf}} \mu_{(0,\omega^2)} < \max_{\omega_{\rm uf}<\omega} \mu_{(0,\omega^2)}.$$

This predicted hierarchy is confirmed by these the simulations considered in Fig. S2,

$$|\delta\varepsilon_{\text{Fig.S2(a)}}|\bar{u}_{\rm lf} < |\delta\varepsilon_{\text{Fig.S2(c)}}|\bar{u}_{\rm uf} < |\delta\varepsilon_{\text{Fig.S2(b)}}|\bar{u}_{\rm uf},$$

where the absolute value of each perturbation strength necessary to annihilate a specified corner-localized mode is scaled by the overlap with that corner-localized mode.

In the numerical results discussed in this section and the main text, the perturbation was chosen to respect the system's reflection symmetry so that the symmetry-reduced spectral localizer remained Hermitian and the topological corner-localized states retained well-defined eigenvalues with respect to $\mathcal{R}_y$. However, it is likely possible to also consider the system's topological protection against perturbations that do not respect reflection symmetry. Of course, in this case, the corner-localized topological state would no longer be either even or odd with respect to the reflection symmetry, but it may be possible to quantitatively predict a perturbation strength below which the state must still exist. Such a prediction may be possible using known results for symmetry-destroying perturbations to systems with strong topology [16], or by considering a non-Hermitian extension of the symmetry-reduced spectral localizer similar to what has been developed for Class A systems [17].

SV. Identifying topological edge-localized states

Re-configuring the corner photonic heterostructure considered in Fig. 1 of the main text so that the mirror symmetry axis intersects an edge rather than a corner, shows that the same local marker and local gap definitions can be used

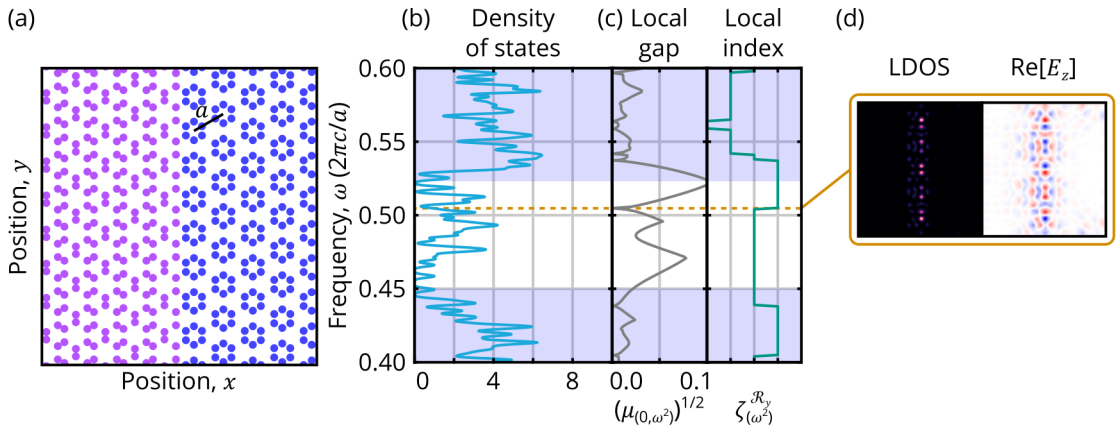

FIG. S3. (a) Diagram of a 2D photonic structure with a straight edge between crystals formed from expanded (purple) and contracted (blue) hexagonal clusters that have the same properties as in Fig. 1 of the main text, bounded by a perfect electric conductor. (b) Density of states for the finite system in (a). (c) Local gap $(\mu_{(0,\omega^2)})^{(1/2)}$ in units of $2\pi c/a$ and local index $\zeta^{\mathcal{R}_y}_{\omega^2}$ calculated using $\kappa = 0.01(2\pi c)^2/a^3$. In (b,c) the shaded regions demarcate those spectral regions where states can exist in the crystalline bulk. (d) LDOS at the frequency of the local gap closing and real part of the E_z field for the mode at $\omega = 0.504(2\pi c/a)$.

to identify topological edge-localized states centered at $y = 0$, see Fig. S3. Indeed, as can be seen, it would be nearly impossible to uniquely identify the topological edge-localized state in this system from its DOS, due to all of the surrounding nearly degenerate states, Fig. S3(b). However, only a single state causes the local gap to close within the heterostructure's bulk band gap, where the topological marker also changes, Fig. S3(c), and this frequency corresponds to a state that is edge-localized, Fig. S3(d). Note that due to the system possessing perfect electric conductor boundaries (open boundaries in the standard language of condensed matter systems), one only expects a small number of edge states to be topological with respect to the reflection symmetry of the system's $y = 0$ axis, as opposed to a number proportional to the length of the edge. To identify the remainder of the edge-localized states, one could instead impose periodic boundaries and define a set of reflection symmetries corresponding to the center and edges of each horizontal ribbon super-cell, similar to what is considered in Ref. [18]. Then, the set of all topological edge-localized states would be the union of all those states identified by each choice of reflection symmetry. Altogether, these simulations demonstrate that the local crystalline topological marker $\zeta^{\mathcal{S}}_E$ is applicable to both first-order and higher-order topology.

SVI. Eigenstates of the symmetry-reduced spectral localizer

In the main text after Eq. (10), it is claimed that the eigenstates of the $\mathcal{R}_y$-reduced spectral localizer at gap-closing are approximately given by eigenstates of the underlying Hamiltonian. In this section, we provide some numerical justification for this claim (as well as the discussion in Sec. SI), but also note that this is still a relatively crude approximation that somehow still results in a prediction, Eq. (12), that is numerically observed to be correct in Fig. 1 in the main text and Fig. S3. As a reminder, we are using $\boldsymbol{\phi}_{\omega^2}$ as the eigenvector of the symmetry-reduced spectral localizer $\tilde{L}^{\mathcal{R}_y}_{\omega^2}$ that corresponds to its smallest eigenvalue at ω. Similarly, the eigenvectors of the Hermitian Hamiltonian generated from Maxwell's equations are $\boldsymbol{\psi} = M^{-1/2}E_z$.

As can be seen in Fig. S4(a),(b), $\boldsymbol{\phi}_{\omega^2}$ is in reasonable agreement with the corresponding eigenstate of H, $\boldsymbol{\psi}_{\mathrm{b}}$ for these corner-localized states. However, note that, as the symmetry-reduced spectral localizer does not commute with the spatial symmetry $\mathcal{S}$, $\boldsymbol{\phi}_{\omega^2}$ is neither even nor odd with respect to this symmetry. For Fig. S4(c), we can see that even though the system's eigenstate is localized to the interface, but still extended along it, $\boldsymbol{\phi}_{\omega^2}$ is localized to the reflection operator's center, i.e., the y-axis. Thus, the spectral localizer can identify topological states even if they are not perfectly localized.

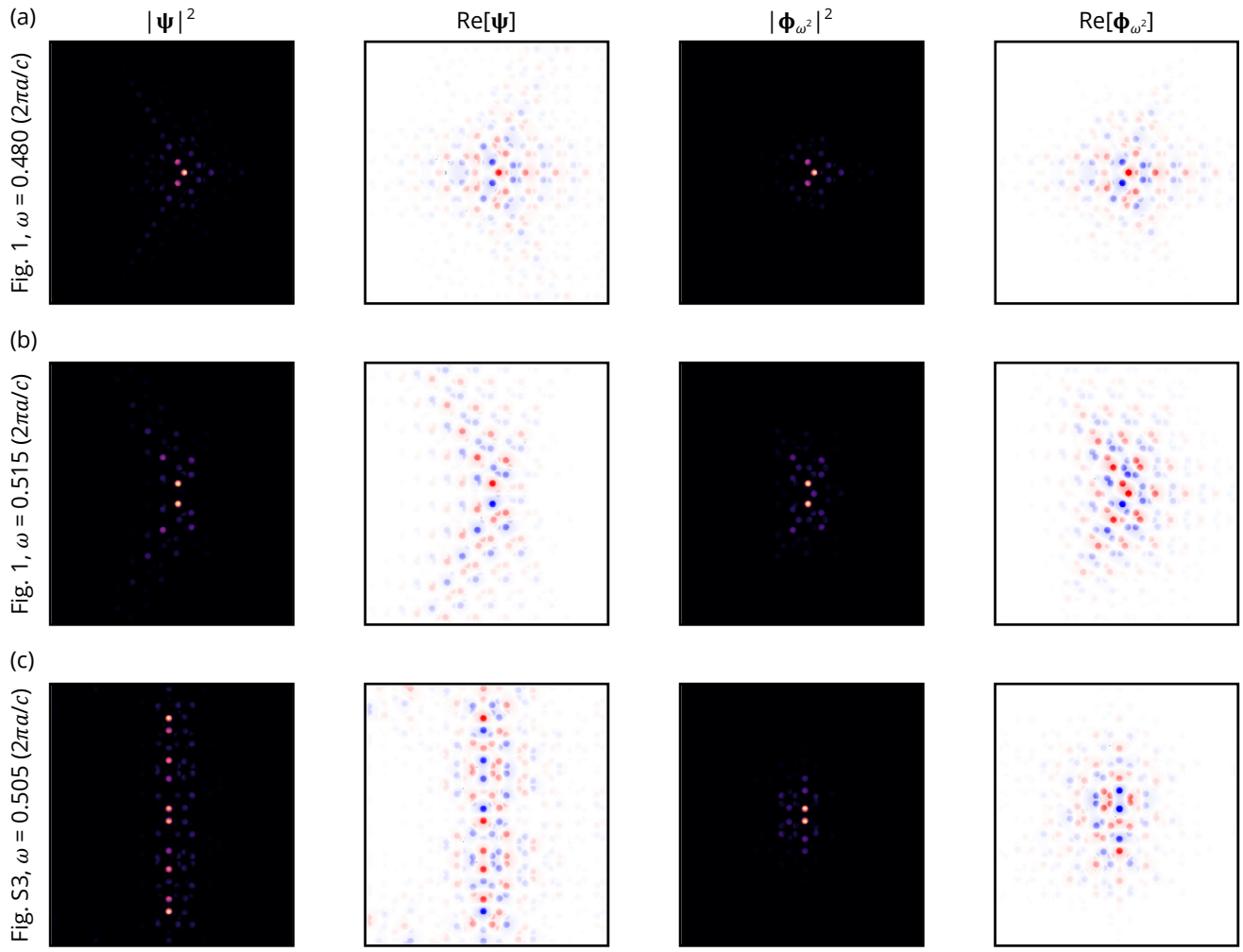

FIG. S4. (a) For the system shown in the main text in Fig. 1, from left to right, the eigenstate intensity $|\psi|^2$ of H whose frequency is $\omega = 0.480(2\pi c/a)$, the corresponding real part of the eigenstate Re[ψ], the squared absolute value $|\phi_{\omega^2}|^2$ of the eigenvector ϕ_{ω^2} of the $\mathcal{R}_y$-reduced spectral localizer whose corresponding eigenvalue is the closest to zero, and Re[ϕ_{ω^2}]. (b) Similar to (a), but for $\omega = 0.515(2\pi c/a)$ from that same system. (c) Similar to (a), but for $\omega = 0.505(2\pi c/a)$ for the system shown in Fig. S3 in the main text. In all cases, $\kappa = 0.01(2\pi c)^2/a^3$.

SVII. Examples of edge-localized states in the corner heterostructure that are trivial with respect to the local index

In the discussion about Fig. 1 in the main text, we claim that the other states seen in the shared bulk band gap of the photonic crystal heterostructure are edge-localized states and not corner-localized states. In Fig. S5 we provide evidence for this claim. As can be seen, for frequencies corresponding to choices where the DOS is non-zero within the bulk band gap, but not frequencies where the local gap closes and the local index changes, the states are edge-localized, not corner-localized.

SVIII. Application of the symmetry-reduced spectral localizer to a tight-binding model

Here, we provide an example of the symmetry-reduced spectral localizer of a tight-binding model that identifies its crystalline topological states. In particular, we choose the "breathing" honeycomb lattice with C_{6v} symmetry shown in Fig. S6(a). This lattice is characterized by two coupling coefficients, the intra–unit cell coupling t_{in}, and the inter–unit cell coupling t_{out}. Here, we set the on-site energies to be zero, so the system also exhibits chiral symmetry. This lattice has been previously studied for its zero-energy states protected by chiral symmetry [19].

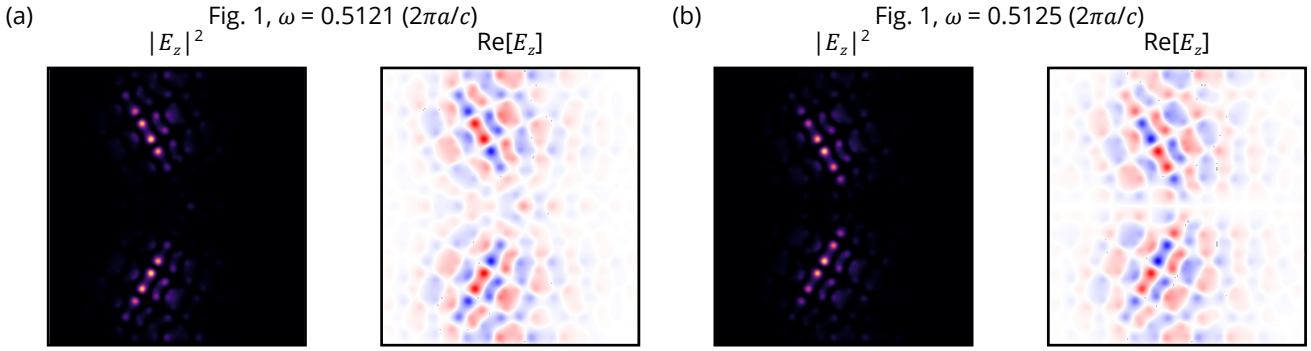

FIG. S5. For the system shown in the main text in Fig. 1, $|E_z|^2$ and Re$[E_z]$ at (a) $\omega = 0.5121(2\pi c/a)$ and at (b) $\omega = 0.5125(2\pi c/a)$.

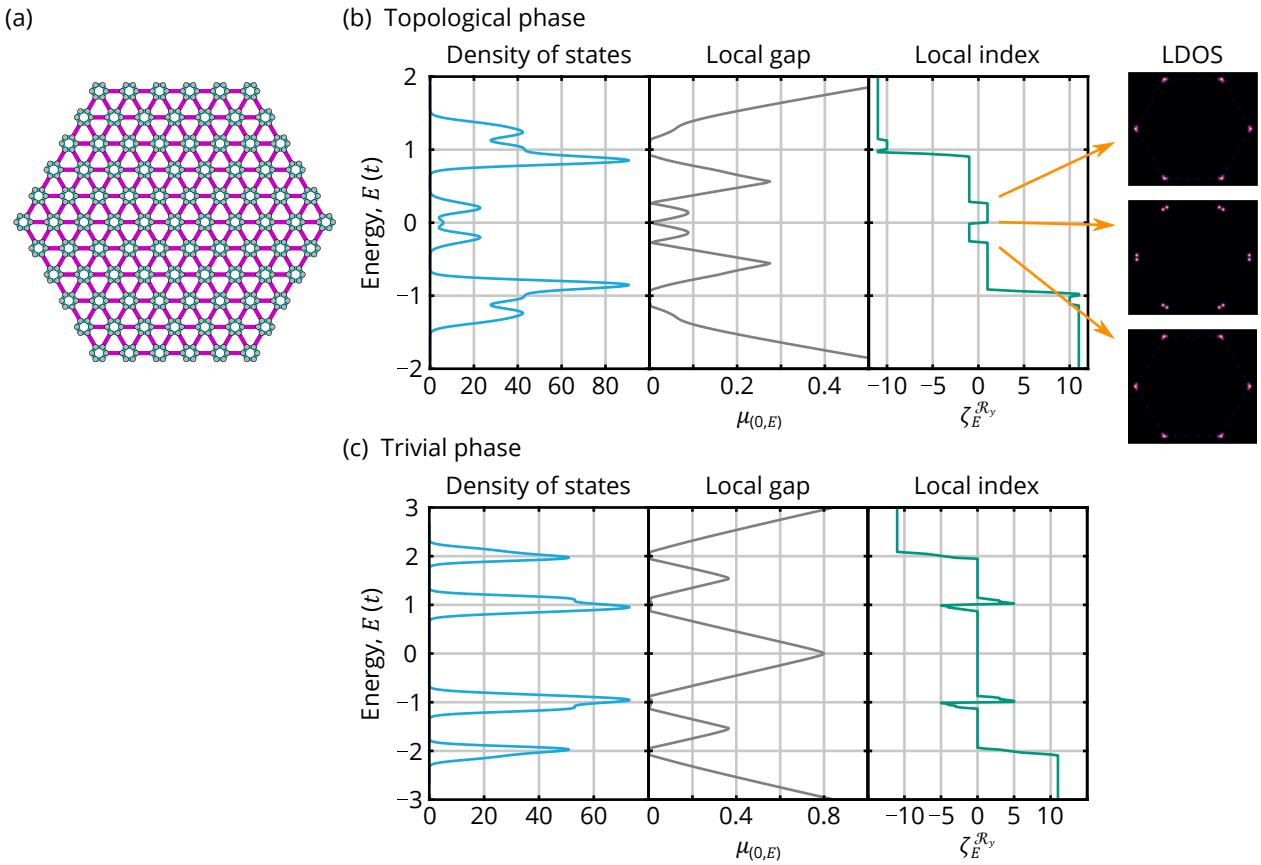

FIG. S6. (a) Schematic of the finite breathing honeycomb lattice with C_{6v} symmetry. The intra–unit cell couplings (t_{in}) are shown in cyan, and the inter–unit cell couplings (t_{out}) are shown in magenta, with lattice constant is a. (b) Density of states, local gap $\mu_{(0,E)}$, and local index $\zeta_E^{\mathcal{R}_y}$ for the breathing honeycomb lattice for $t_{\text{in}} = 0.2t$ and $t_{\text{out}} = t$. The local density of states (LDOS) is shown for the three in-gap energies where the topological index is seen to change. (c) Similar to (b), except for $t_{\text{in}} = t$ and $t_{\text{out}} = 0.2t$. For (b),(c), $\kappa = 0.1(t/a)$.

Instead, here we analyze the breathing honeycomb lattice using the symmetry-reduced spectral localizer. Again, we choose $\mathcal{S} = \mathcal{R}_y$, the reflection symmetry about the system's $y = 0$ axis, yielding the local index $\zeta_E^{\mathcal{R}_y}$ and local gap $\mu_{(0,E)}$ as defined in the main text. When, $t_{\text{out}} > t_{\text{in}}$ [Fig. S6(b)], the system exhibits three in-gap index switches, showing that the system's topology is changing at these energies. The local density of states (LDOS) reveals that all three of these switches correspond to corner-localized states. In contrast, when $t_{\text{in}} > t_{\text{out}}$ [Fig. S6(c)], there are no in-gap topological index changes, only changes that occur within the spectral extent of the system's bulk bands.

Note that the system's local index in the topological phase only changes by 2 at the energy of each set of corner states, not 6, despite there being six corners. This is because only two of the corner states are topological with respect to $\mathcal{R}_y$ — the other four corner states are topological with respect to the two reflection axes that bisect those corners. Similarly, the index is changing by 2, rather than 1, because each reflection axis is bisecting two corners on opposite sides of the lattice. In contrast, in Fig. 1 of the main text, the system only has a single corner along the reflection symmetry's axis.

[1] T. A. Loring and H. Schulz-Baldes, Finite volume calculation of K-theory invariants, New York J. Math. **23**, 1111 (2017).
[2] T. A. Loring and H. Schulz-Baldes, The spectral localizer for even index pairings, J. Noncommut. Geom. **14**, 1 (2020).
[3] H. Schulz-Baldes and T. Stoiber, The spectral localizer for semifinite spectral triples, Proceedings of the American Mathematical Society **149**, 121 (2021).
[4] N. Doll, H. Schulz-Baldes, and N. Waterstraat, *Spectral Flow: A Functional Analytic and Index-Theoretic Approach*, Vol. 94 (Walter de Gruyter GmbH & Co KG, 2023).
[5] T. Kato, *Perturbation theory for linear operators*, Vol. 132 (Springer Science & Business Media, 2013).
[6] W. Cheng, A. Cerjan, S.-Y. Chen, E. Prodan, T. A. Loring, and C. Prodan, Revealing topology in metals using experimental protocols inspired by K-theory, Nat. Commun. **14**, 3071 (2023).
[7] H. Lin, Almost commuting selfadjoint matrices and applications, in *Operator algebras and their applications (Waterloo, ON, 1994/1995)*, Fields Inst. Commun., Vol. 13 (Amer. Math. Soc., Providence, RI, 1997) pp. 193–233.
[8] M. B. Hastings, Topology and phases in fermionic systems, J. Stat. Mech , L01001 (2008).
[9] T. A. Loring and A. P. Sørensen, Almost commuting unitary matrices related to time reversal, Communications in Mathematical Physics **323**, 859 (2013).
[10] T. A. Loring and A. P. Sørensen, Almost commuting self-adjoint matrices: the real and self-dual cases, Reviews in Mathematical Physics **28**, 1650017 (2016).
[11] N. Doll and H. Schulz-Baldes, Skew localizer and $\mathbb{Z}_2$-flows for real index pairings, Advances in Mathematics **392**, 108038 (2021).
[12] A. P. Schnyder, S. Ryu, A. Furusaki, and A. W. W. Ludwig, Classification of topological insulators and superconductors in three spatial dimensions, Phys. Rev. B **78**, 195125 (2008).
[13] A. Kitaev, Periodic table for topological insulators and superconductors, AIP Conference Proceedings **1134**, 22 (2009).
[14] S. Ryu, A. P. Schnyder, A. Furusaki, and A. W. W. Ludwig, Topological insulators and superconductors: tenfold way and dimensional hierarchy, New Journal of Physics **12**, 065010 (2010).
[15] K. Y. Dixon, T. A. Loring, and A. Cerjan, Classifying Topology in Photonic Heterostructures with Gapless Environments, Phys. Rev. Lett. **131**, 213801 (2023).
[16] N. Doll and H. Schulz-Baldes, Approximate symmetries and conservation laws in topological insulators and associated $\mathbb{Z}$-invariants, Ann. Physics **419**, 168238, 25 (2020).
[17] A. Cerjan, L. Koekenbier, and H. Schulz-Baldes, Spectral localizer for line-gapped non-hermitian systems, Journal of Mathematical Physics **64**, 082102 (2023).
[18] S. Velury, B. Bradlyn, and T. L. Hughes, Topological crystalline phases in a disordered inversion-symmetric chain, Phys. Rev. B **103**, 024205 (2021).
[19] J. Noh, W. A. Benalcazar, S. Huang, M. J. Collins, K. P. Chen, T. L. Hughes, and M. C. Rechtsman, Topological protection of photonic mid-gap defect modes, Nat. Photonics **12**, 408 (2018).